TOWARD IDENTIFYING THE UNASSOCIATED GAMMA-RAY SOURCE 1FGL J1311.7-3429 WITH X-RAY AND OPTICAL OBSERVATIONS

J. KATAOKA[1], Y. YATSU[2], N. KAWAI[2], Y. URATA[3], C. C. CHEUNG[4,7], Y. TAKAHASHI[1], K. MAEDA[1], T. TOTANI[5],
R. MAKIYA[5], H. HANAYAMA[6], T. MIYAJI[6], AND A. TSAI[3]

[1] Research Institute for Science and Engineering, Waseda University, 3-4-1, Okubo, Shinjuku, Tokyo 169-8555, Japan; kataoka.jun@waseda.jp
[2] Tokyo Institute of Technology, 2-12-1, Ohokayama, Meguro, Tokyo 152-8551, Japan
[3] Institute of Astronomy, National Central University, Chung-Li 32054, Taiwan
[4] National Research Council Research Associate, National Academy of Sciences, Washington, DC 20001, USA
[5] Department of Astronomy, Kyoto University, Kitashirakawa, Sakyo-ku, Kyoto 606-8502, Japan
[6] Ishigakijima Astronomical Observatory, National Astronomical Observatory of Japan, 1024-1 Arakawa, Ishigaki, Okinawa, 907-0024, Japan

ABSTRACT

We present deep optical and X-ray follow-up observations of the bright unassociated *Fermi*-LAT gamma-ray source 1FGL J1311.7-3429. The source was already known as an unidentified EGRET source (3EG J1314-3431, EGR J1314-3417), hence its nature has remained uncertain for the past two decades. For the putative counterpart, we detected a quasi-sinusoidal optical modulation of $\Delta m \sim 2$ mag with a period of $\simeq 1.5$ hr in the Rc, r', and g' bands. Moreover, we found that the amplitude of the modulation and peak intensity changed by $\gtrsim 1$ mag and ~ 0.5 mag, respectively, over our total six nights of observations from 2012 March to May. Combined with *Swift* UVOT data, the optical–UV spectrum is consistent with a blackbody temperature, $kT \simeq 1$ eV and the emission volume radius $R_{bb} \simeq 1.5 \times 10^4 \, d_{kpc}$ km (d_{kpc} is the distance to the source in units of 1 kpc). In contrast, deep *Suzaku* observations conducted in 2009 and 2011 revealed strong X-ray flares with a light curve characterized with a power spectrum density of $P(f) \propto f^{-2.0 \pm 0.4}$, but the folded X-ray light curves suggest an orbital modulation also in X-rays. Together with the non-detection of a radio counterpart, and significant curved spectrum and non-detection of variability in gamma-rays, the source may be the second "radio-quiet" gamma-ray emitting millisecond pulsar candidate after 1FGL J2339.7-0531, although the origin of flaring X-ray and optical variability remains an open question.

Key words: gamma rays: stars – pulsars: general – X-rays: general

Online-only material: color figures

1. INTRODUCTION

The Large Area Telescope (LAT; Atwood et al. 2009) on board the *Fermi Gamma-Ray Space Telescope* is a successor to EGRET on board the *Compton Gamma-Ray Observatory* (Hartman et al. 1999), with much improved sensitivity, resolution, and energy range. The second *Fermi*-LAT catalog, based on the first 24 months of all-sky survey data (2FGL; Nolan et al. 2012), provides source location, flux, and spectral information, as well as light curves on month time bins for 1873 γ-ray sources detected and characterized in the 100 MeV–100 GeV range. Thanks to their small localization error circles (or ellipses) with typical 95% confidence radii, $r_{95} \simeq 0°\!.1$–$0°\!.2$, for relatively bright sources, 69% of the 2FGL sources are reliably associated or firmly identified with counterparts of known or likely γ-ray producing sources. In particular, more than 1000 sources are proposed to be associated with active galactic nuclei (AGNs; of mainly the blazar class) and 87 sources with pulsars (PSRs), including 21 millisecond pulsars (MSPs), which are a new category of γ-ray sources discovered with *Fermi*-LAT (Nolan et al. 2012; Abdo et al. 2009a). Other sources, albeit of a relative minority compared to AGNs and PSRs, also constitute important categories of new GeV sources like supernova remnants (SNRs; Abdo et al. 2009b, 2010a, 2010b, 2010c), low-mass/high-mass binaries (Abdo et al. 2009c, 2009d, 2009e), pulsar wind nebula (Abdo et al. 2010d, 2010e), one nova (Abdo et al. 2010f),

normal and starburst galaxies (Abdo et al. 2010g, 2010h), and the giant lobes of a radio galaxy (Abdo et al. 2010i).

Despite such great advances in the identification of *Fermi*-LAT sources, 575 (31%) sources in the 2FGL catalog still remain unassociated. Note that a substantial fraction of the unassociated sources (51%) have at least one analysis flag due to various issues, while only 14% of the associated sources have been flagged (Nolan et al. 2012). This may suggest that some of unassociated sources are spurious due to complexity/difficulty of being situated in a crowded region near the Galactic plane. Nevertheless, many of them are bright enough to be listed in the one year *Fermi*-LAT catalog (1FGL; Abdo et al. 2010j) and some of them are even listed in the bright source list based on the first 3 months of data (0FGL; Abdo et al. 2009f). By comparing the distribution of associated and unassociated sources in the sky, a number of interesting features in the map were reported (Nolan et al. 2012). For example, (1) the number of unassociated sources decreases with increasing Galactic latitude, (2) the number of unassociated sources increases sharply below Galactic latitudes, $|b| < 10°$, and (3) the fraction of sources with curved gamma-ray spectra among the unassociated sources is greater (28%) than the fraction of curved spectra sources among the associated sources (16%). Further extensive studies based on a statistical approach in an effort to correlate their gamma-ray properties with the AGN and PSR populations was presented for 1FGL unassociated sources (Ackermann et al. 2012).

In this context, 1FGL J1311.7-3429 (or 2FGL name, 2FGL J1311.7-3429) is a *classical* unassociated gamma-ray

---

[7] Resident at Naval Research Laboratory, Washington, DC 20375, USA.

source situated at high Galactic latitude ($l = 307°.6859$, $b = 28°.1951$), and was first discovered by EGRET about 20 years ago as 3EG J1314-3431 (Hartman et al. 1999) or EGR J1314-3417 (Casandjian & Grenier 2008). The source was also reported by *Fermi*-LAT in the 0FGL list with a gamma-ray flux $F_{0.1-20\,\mathrm{GeV}} = (11.7 \pm 1.1) \times 10^{-8}$ photons cm^{-2} s^{-1}, which is marginally consistent with the gamma-ray flux determined by EGRET, $F_{0.1-20\,\mathrm{GeV}} = (18.7 \pm 3.1) \times 10^{-8}$ photons cm^{-2} s^{-1}, within the 2σ level. In the 2FGL catalog, the detected significance of 1FGL J1311.7-3429 is 43.1σ, which is one of the brightest sources with an UNID flag. Based on the one-month binned >100 MeV gamma-ray light curve of 1FGL J1311.7-3429 over two years of data as published in the 2FGL catalog,[8] no statistically significant variability was observed (VARIABILITY_INDEX = 19.09; Nolan et al. 2012). The gamma-ray spectrum is significantly curved with curved significance SIGNIF_CURVE of 6.33 (Nolan et al. 2012).[9]

The first X-ray follow-up observation of 1FGL J1311.7-3429 was conducted as a part of *Suzaku* X-ray observations of 11 unidentified *Fermi*-LAT objects at high Galactic latitude, $|b| > 10°$ (Maeda et al. 2011; Takahashi et al. 2012). The X-ray source associated with 1FGL J1311.7-3429 showed a very rapid X-ray flare with the count rate changing by a factor of 10. Subsequent *Chandra* ACIS-I (2010 March 21 for a 19.87 ks exposure, obsID 11790) and *Swift* XRT observations (2009 February 27 for a 3.34 ks exposure, obsID 31358; see also Table 1) confirmed that the brightest X-ray source within the *Fermi*-LAT error ellipse is the most credible counterpart and that the X-ray source is also variable on month-to-year timescales. The unabsorbed X-ray flux observed with *Chandra* was 1.03×10^{-13} erg cm^{-2} s^{-1} in the 0.5–8 keV band, with a differential photon spectral index, $\Gamma = 1.26^{+0.38}_{-0.37}$ (Cheung et al. 2012).

Motivated by the initial X-ray results, we conducted further deep observations of 1FGL J1311.7-3429 with *Suzaku*, together with deep optical observations using a 105 cm Ritchey–Chrétien telescope (g', Rc, and Ic bands) at the Ishigakijima Astronomical Observatory (IAO) in Japan, as well as the 1 m telescope (r' band) at Lulin Observatory in Taiwan. In Section 2, we describe the details of the *Suzaku* observations and optical observations and data reduction procedures. Very recently, Romani (2012) reported quasi-sinusoidal optical modulation of this source with a 1.56 hr (5626 s) period, suggesting that the source is another black-widow-type MSP like that recently discovered for 1FGL J2339.7-0531 (Romani & Shaw 2011; Kong et al. 2012). Our paper confirms some of those optical findings for 1FGL J1311.7-3429, plus provides results from multiple epoch optical monitoring between 2012 March and May and completely new X-ray data based on a long *Suzaku* observation conducted in 2011 together with our previously published archival 2009 data. The results of these observations are given in Section 3. Based on our new observational data in optical and X-ray, and various observed gamma-ray parameters compiled in the 2FGL source catalog, we support that 1FGL J1311.7-3429 could be a "radio-quiet" gamma-ray emitting MSP candidate
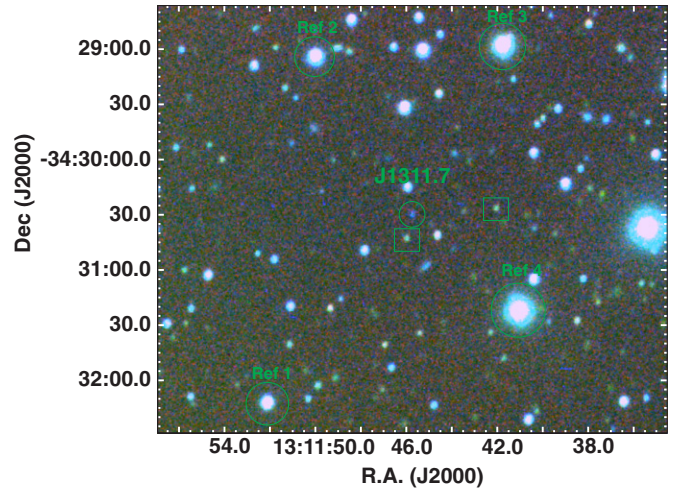
Figure 1. Tri-color optical image of 1FGL J1311.7-3429 constructed from data taken in the g', Rc, and Ic bands by the IAO 1.05 m telescope (Table 1). The four reference stars used in the analysis of the IAO data are denoted as Ref 1–4, while two reference stars used in the analysis of the LOT data are shown as boxes.
(A color version of this figure is available in the online journal.)

like 1FGL J2339.7-0531. The variable optical/X-ray source is posited as the counterpart to the gamma-ray source and throughout, we refer to it simply as 1FGL J1311.7-3429.

2. OBSERVATIONS AND DATA REDUCTION

2.1. Optical/UV

As discussed in Cheung et al. (2012), the brightest X-ray source within the *Fermi*-LAT error ellipse, CXOU J131145.71-343030.5, is the most credible counterpart and exactly the one detected in our previous (AO4; below) *Suzaku* observation (Maeda et al. 2011). The source was also detected with the *Swift* XRT (observation ID 31358). Within the *Chandra* error circle (0″.6 at 90% level), there is a $R = 17.9$ mag, $B = 20.5$ mag star in the USNO A-2.0 catalog (Muslimov & Harding 2003), that is 0″.56 apart from CXOU J131145.71-343030.5. The same star is also listed as $R = 18.8$ mag, $B = 21.0$ mag in USNO-B1.0 catalog, suggesting a hint of temporal variability (a typical uncertainty of these measurements is $\simeq 0.3$ mag; Muslimov & Harding 2003). The same optical source is also seen in the DSS (Digital Sky Survey), but its optical magnitude is unclear. Moreover, *Swift* UVOT observations taken simultaneously with the XRT detected the source. Our analysis using archival *Swift* UVOT data indicate: $v > 19.51$ (upper limit only), $b = 20.10 \pm 0.30$, $u = 20.77 \pm 0.27$, $uvw1 = 21.70 \pm 0.31$, $uvm2 = 21.58 \pm 0.24$, and $uvw2 = 22.05 \pm 0.22$.

We made further deep follow-up observations of the field of CXOU J131145.71-343030.5, centered at (R.A., decl.) = (197°.940400, $-34°.508306$), with the 105 cm Ritchey–Chrétien telescope at the Ishigakijima Astronomical Observatory in Japan. These observations were obtained on 2012 May 25 and started at 12:31:11:13 and ended 15:41:11:63 (UT). The telescope in IAO is equipped with a tricolor camera that performs simultaneous imaging in the SDSS-g' (hereafter, g'), Rc and Ic bands. The total net exposure amounts to 8400 s (300 s × 28 frames; see Table 1 for the observation log). All images were flat field and bias corrected. The absolute magnitudes were calibrated against the four reference stars shown in Figure 1. In the Rc and Ic bands, the reference star

---

[8] http://heasarc.gsfc.nasa.gov/FTP/fermi/data/lat/catalogs/source/lightcurves/2FGL_J1311d7m3429_lc.png
[9] As detailed in Nolan et al. (2012), the VARIABILITY_INDEX is an indicator of the flux being constant across the full 2 year period. A value of VARIABILITY_INDEX > 41.6 is used to identify variable sources at a 99% confidence level. Similarly, the SIGNIF_CURVE parameter is an indicator of the spectrum being curved, by comparing the likelihood values calculated for a LogParabola and a single power-law function. SIGNIF_CURVE is distributed as χ^2 with 1 degree of freedom, and SIGNIF_CURVE > 16 corresponds to 4σ significance of curvature.

Table 1
Observation Log of 1FGL J1311.7−3429 Analyzed in This Paper

Obs Start (UT)	Obs End (UT)	Observatory	Band	Exposure
2009-08-04 04:56:35	2009-08-05 07:18:14	*Suzaku* XIS	X-ray	33.0 ks
2011-08-01 16:48:20	2011-08-03 17:40:15	*Suzaku* XIS	X-ray	65.2 ks
2009-02-27 18:41:59	2009-02-27 22:04:57	*Swift* UVOT	UV	276/276/276/552/742/1106[a]
2012-03-24 17:45:37	2012-03-24 19:38:35	LOT 1 m	r'	5 min × 21
2012-03-25 17:48:26	2012-03-25 19:26:33	LOT 1 m	r'	5 min × 12
2012-03-26 17:25:14	2012-03-26 18:29:59	LOT 1 m	r'	5 min × 12
2012-04-12 16:35:08	2012-04-12 18:24:30	LOT 1 m	r'	5 min × 21
2012-05-24 13:00:49	2012-05-24 15:34:44	LOT 1 m	r'	5 min × 29
2012-05-25 12:31:11	2012-05-25 15:41:11	IAO 105 cm	g', Rc, Ic	20 min × 7

Note. [a] *Swift* UVOT exposures for the $v/b/u/uvw1/uvm2/uvw2$ bands in seconds.

magnitudes were based on the NOMAD catalog (Monet et al. 2003). Because the target area was not covered by the SDSS, we employed a system conversion formula of USNO-B Bc and Rc magnitudes (Sesar et al. 2006) for the four reference stars to obtain g' magnitudes. Moreover, the observed magnitudes were corrected for Galactic extinction using $A_{g'} = 0.247$ mag, $A_{Rc} = 0.167$ mag, and $A_{Ic} = 0.120$ mag.

We also conducted optical SDSS-r' (hereafter r') band monitoring observations with the Lulin One-meter Telescope (LOT; Huang et al. 2005). Observations were conducted on five nights between 2012 March and May (see Table 1). Photometric images with 300 s exposure were obtained using the PI1300B CCD camera. We performed the dark-subtraction and flat-fielding correction using the appropriate calibration data. For these LOT data, the four reference stars used in the IAO photometry were saturated in the detector and therefore could not be used. Instead, the LOT photometric results are presented as differential magnitudes against two other fainter reference stars (boxed in Figure 1).

2.2. Suzaku XIS

As noted above, the first X-ray follow-up observation of 1FGL J1311.7−3429 was conducted in 2009 as a part of AO-4 *Suzaku* program (PI: J. Kataoka; OBS_ID 804018010) aimed at observing an initial four out of 11 unidentified *Fermi*-LAT objects at high Galactic latitude, $|b| > 10°$ (Maeda et al. 2011; see also Takahashi et al. 2012). To further investigate the nature of the detected variable X-ray counterpart, we conducted the second *Suzaku* observation of 1FGL J1311.7−3429 in 2011 as a part of AO-6 program (PI: J. Kataoka, OBS_ID 706001010). The observation started at 2011 August 1 16:48:20 and ended at August 3 17:40:15. The total exposure amounted to 65.2 ks, and is almost twice as long as that obtained in AO-4 (see Table 1). For both the AO-4 and AO-6 data analysis, we excluded the data collected during the time and up to 60 s after the South Atlantic Anomaly (SAA), and excluded data corresponding to less than 5° of the angle between Earth's limb and the pointing direction. Moreover, we excluded time windows during which the spacecraft was passing through the low cutoff rigidity (COR) of below 6 GV. We set the same source region to within a 1′ radii around the respective X-ray flux maximum and the selection criteria for the data analysis for the two data sets were completely the same. Although *Suzaku* also carries a hard X-ray detector (HXD), consisting of the PIN and GSO, hereafter, we do not use the data because the source is too faint to be detected with HXD/PIN or GSO.

3. RESULTS

3.1. Optical/UV

Figure 1 shows a multicolor image of 1FGL J1311.7−3429 constructed from the IAO g' (blue), Rc (green), and Ic (red) data from 2012 May 24. The optical counterpart of the X-ray source is clearly detected in the image, but apparently the source is rather "blue" compared with reference stars and nearby galaxies. Aperture photometry yielded average magnitudes of the source, $g' = 20.97 \pm 0.13$, $Rc = 21.17 \pm 0.16$, and $Ic < 18.38$ (3σ upper limit). We also checked the temporal profile of the optical emission for the IAO data (Figure 2). Relative photometry for the IAO images against the four field stars shows large amplitude ($\Delta m \sim 2$ mag) quasi-sinusoidal modulation in the g' and Rc bands with a timescale of 1.5 hr, as suggested by Romani (2012).

To search for possible long-term variability, Figure 3 (top) compares the r'-band light curve reconstructed only from LOT data between 2012 March and May. The differential magnitudes are derived by comparison with two reference stars in the field (see Figure 1). Note, the r'-band magnitude of the reference stars remain constant within $\Delta m = 0.068$ mag over the five nights of observations. Interestingly, the amplitude of modulation and the light-curve profile seems to have changed among the five nights of observations. Specifically, a clear modulation of $\Delta m \sim 2$ mag is visible in the May 24 data, while $\Delta m \sim 1$ mag in the March 24 data, and almost unseen ($\Delta m \lesssim 0.2$ mag) in the March 26 data. Moreover, the peak magnitude differs by $\Delta m \sim 0.5$ mag among the five nights, much larger than the fluctuations in the magnitudes of reference stars. Figure 3 (bottom) shows the folded light curves of differential r'-band magnitudes with a best-fit period of 1.56278 hr (5626 s) proposed by Romani (2012). Phase zero is defined here as MJD 56010.76808, so that the time of the observed minimum r'-band magnitude in the May 24 data is set at orbital phase $\phi = 1.0$. The peak r'-band magnitude is around $\simeq 20.5$ for five nights of data from 2012 March to April. Note, this is exactly consistent with what has been observed with IAO on May 25 (Figure 2, right). To further investigate the temporal variability/flaring in the UV data, we also reanalyzed the archival *Swift* UVOT data. However, the UVOT exposures for each filter (b, u, $uvw1$, $uvm2$, $uvw2$) were too short to search for variability (see Table 1).

3.2. Suzaku XIS

During the AO-4 observation, significant X-ray variability was detected at the beginning of the observation, where the count rate changed by a factor of 10 (Maeda et al. 2011). Figure 4 compares the *Suzaku* XIS FI (XIS0+3) images in
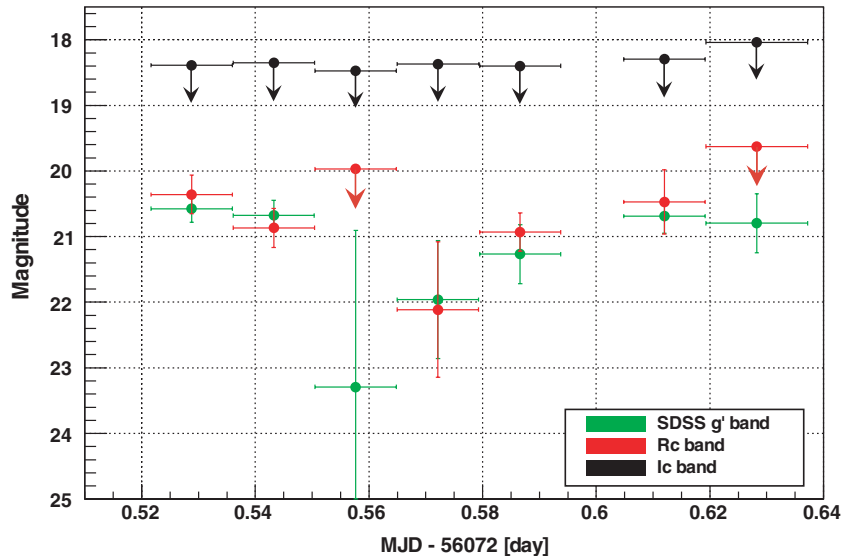
Figure 2. Multi-band optical light curves of 1FGL J1311.7-3429 observed with the IAO 1.05 m telescope on May 25 (g', Rc, and Ic bands). Data are binned by 1200 s (300 s $\times$ 4 frames) for the IAO data. The source is not detected in the Ic band and 3σ upper limits are provided.

(A color version of this figure is available in the online journal.)

the 0.5–10 keV range, reconstructed by using the data during the first 20 ks (top) and the last 74 ks (bottom). The images are corrected for exposure and vignetting, and are non-X-ray (detector) background subtracted. The images were also smoothed by a Gaussian function with $\sigma = 0\farcs17$, following the procedure given in Maeda et al. (2011). Note that the source is clearly detected in the first 20 ks, but almost unseen in the last 74 ks. Also Cheung et al. (2012) argues that the 0.3–10 keV *Swift* XRT count rate of $(6.1 \pm 1.8) \times 10^{-3}$ counts s^{-1} is equivalent to a 0.5–8 keV flux of $\simeq 3.1 \times 10^{-13}$ erg cm^{-2} s^{-1}, indicating a $\sim 3\times$ brighter source about one year prior to the *Chandra* observation, and providing further evidence of long-term X-ray variability in this source.

Figure 5 summarizes the X-ray light curve of 1FGL J1311.7-3429 thus obtained during the AO-6 observation and compares them with those obtained in the AO-4 observation. All the XIS0, 1, 3 count rates are summed in the various energy bands of 0.4–1 keV, 1–2 keV, 2–4 keV, and 4–8 keV (from top to bottom). Note that X-ray variability is clearly seen above 1 keV, but not in the 0.4–1 keV light curve. To see this more quantitatively, we calculated the normalized excess variance $\sigma^2_{\rm NXS}$ (Vaughan et al. 2003; see also Kataoka et al. 2007) for the AO4 and AO6 light curves and for the combined AO4+AO6 light curves. The $\sigma^2_{\rm NXS}$ parameter is an estimator of the intrinsic source variance after subtracting the contribution expected from measurement errors. As shown in Figure 6 (top), $\sigma^2_{\rm NXS}$ is consistent with zero for the 0.4–1 keV band, while almost constant (within error bars) and significantly positive above 1 keV.[10]

Figure 6 (bottom) presents the normalized power spectrum density (NPSD; Hayashida et al. 1998), which is a technique for calculating the PSD of unevenly sampled light curves. Note that data gaps are unavoidable for low Earth orbit X-ray satellites like *Suzaku*. Since the orbital period of *Suzaku* is $\sim$5760 s, Earth occultations create artificial periodic gaps every 5760 s in

the data, even when the source is continuously monitored. To calculate the NPSD of our data sets, we made light curves of two different bin sizes of 256 s and 5760 s for each of the AO4 and AO6 light curves (Kataoka et al. 2001). The NPSD calculated for each light curves is well represented by a steep power law with $P(f) \propto f^{-2.00 \pm 0.32}$ (AO4) and $P(f) \propto f^{-2.04 \pm 0.44}$ (AO6). Note that the amplitude of the NPSD is larger for the AO4 (red) data than in the AO6 (blue) data. This is due to large flare observed in the first 20 ks of the AO4 observation (Figure 4) and is consistent with the larger value of $\sigma^2_{\rm NXS}$ compared with variability during AO6 observation (Figure 6, top).

Figure 7 shows the folded X-ray light curves from the *Suzaku* AO4 (top) and AO6 (bottom) data sets. The XIS0, 1, and 3 data are all summed in 0.4–10 keV band. The phase zero is defined as MJD 56010.76808 as in the optical folded light curves shown in Figure 3 (bottom). The vertical axis represents the source counts divided by the average source intensity in the frame. Although there is a regular exposure gap for phases $\phi = 0.3$–0.4 due to Earth occultations, there appears to be a clear excess at phases $\phi = 0.4$–0.6 in AO4 data (see also Romani (2012)). Moreover, we found similar structure in the AO6 data, but at different phases of $\phi = 0.6$–0.8 with much smaller amount of excess. To check that this excess is *not* due to artifacts caused by periodic gaps due to Earth occultation, we also made the folded light curves of the nearby X-ray source in the same field of view (src B in Maeda et al. 2011, or CXOU J131147.0-343205 in Cheung et al. 2012; see Figure 4), whose X-ray flux is comparable to the average X-ray flux of 1FGL J1311.7-3429. The results presented as dashed lines in Figure 7 show no clear excess for the nearby source. This suggests that the X-ray excesses in the folded light curves are most likely due to orbital motion of 1FGL J1311.7-3429 itself.

Finally, Figure 8 compares the unfolded X-ray spectrum for 1FGL J1311.7-3429 averaged over the AO4 (red) and AO6 (blue) observations. The best model fits for both observations consist of power-law continua with photon indices, $\Gamma \simeq 1.3$–1.7. Significant curvature (or deficit of photons below 2 keV) was observed only in the 2009 data, which was tentatively modeled by an excess value of Galactic column density $N_{\rm H}$; $N_{\rm H}$ is,

---

[10] The fractional root mean square variability amplitude, $F_{\rm var}$ is often chosen in preference to $\sigma^2_{\rm NXS}$, although the two convey exactly the same information. Here, we prefer $\sigma^2_{\rm NXS}$ simply because variability is not significant for the 0.4–1 keV light curve and negative values of $\sigma^2_{\rm NXS}$ are possible.
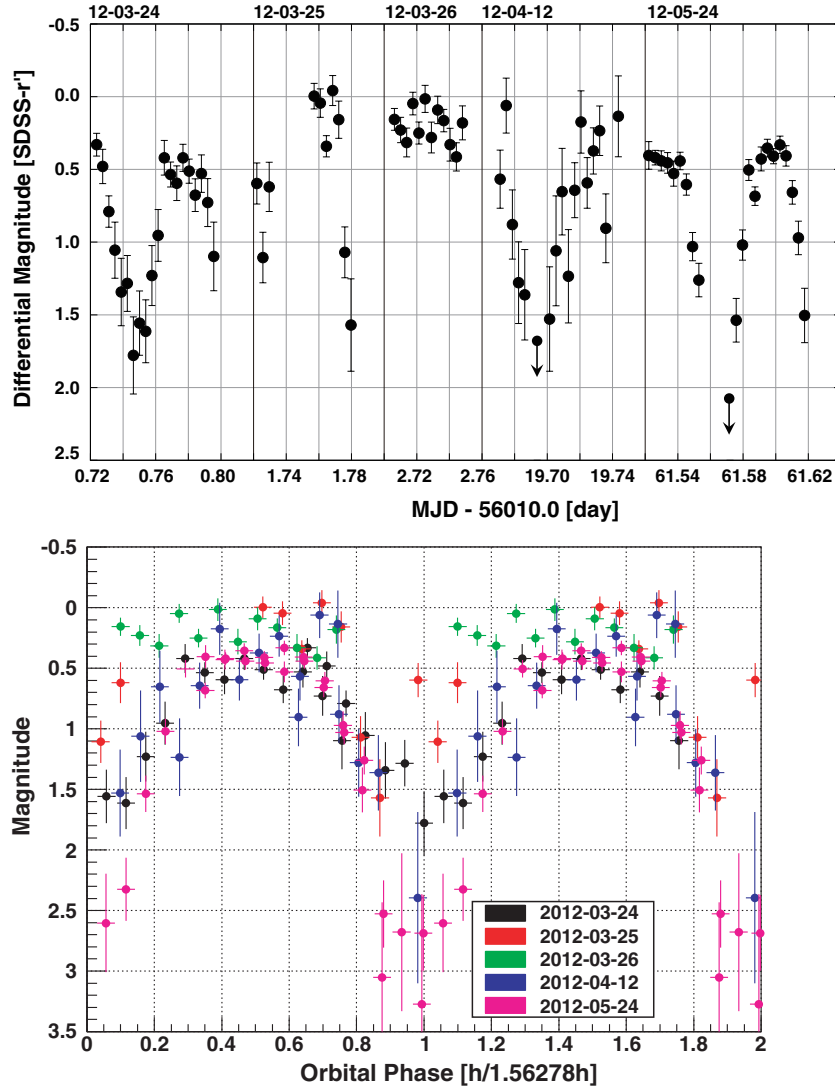
Figure 3. (Top) Temporal variations in the differential r'-band magnitudes derived by comparison with a reference star in the field, observed with the Lulin 1 m telescope from 2012 March to May. The r'-band magnitude of reference star remains constant within $\Delta m = 0.068$ mag. Note that the modulation profile differs largely among five nights of observations. (Bottom) Folded light curve of the differential r'-band magnitudes with a best-fit period of 1.56278 hr (5626 s) proposed by Romani (2012). The phase zero is defined as MJD 56010.76808. Note that both the amplitude of the modulation and the peak intensity changed by $\gtrsim 1$ mag and ~ 0.5 mag, respectively, over the five nights of observations.

(A color version of this figure is available in the online journal.)

Table 2
Fitting Parameters of *Suzaku* Data for the Power-law Model

| Parameter	AO4 Value and Errors[a]	AO6 Value and Errors[a]
$N_{\rm H}$ (10^{20} cm^{-2})	$0.33^{+0.15}_{-0.13}$	<0.07
Γ	$1.71^{+0.18}_{-0.17}$	$1.26^{+0.08}_{-0.07}$
Flux (0.5–2 keV)[b]	$0.99^{+0.27}_{-0.19}$	$0.83^{+0.08}_{-0.06}$
Flux (2–10 keV)[b]	$1.78^{+0.16}_{-0.15}$	2.96 ± 0.15
χ^2 (dof)	17.4 (15)	17.6 (15)
$P(\chi^2)$	0.29	0.29

Notes.
[a] All errors are 1σ.
[b] In unit of 10^{-13} erg cm^{-2} s^{-1}.

however, consistent with zero for the 2011 data. The model fitting results are summarized in Table 2. Although the nearby X-ray source (src B in Maeda et al. 2011, or CXOU J131147.0-343205 in Cheung et al. 2012; see Figure 4) is located only

$1\farcm6$ apart to the south, contamination from this source and other nearby faint sources is estimated to be less than 5% for the applied region of interest of $1'$.

4. DISCUSSION AND CONCLUSIONS

During the first (AO4; 2009) and second (AO6; 2011) *Suzaku* observations, we detected significant variability in 1FGL J1311.7-3429 characterized by repeated flaring activity, with a timescale of $\sim$10 ks. The variability is only clearly seen above 1 keV. The NPSD is well characterized by $P(f) \propto f^{-2}$, as is the case for the X-ray variability of various classes of AGNs including Seyferts and blazars (e.g., Hayashida et al. 1998; Vaughan et al. 2003). The latter class constitutes the majority of *Fermi*-LAT sources but the X-ray variability timescales of blazars are in general somewhat longer, typically $\simeq$1 day (e.g., Kataoka et al. 2001). Such "red-noise" PSD behavior is also observed in X-ray (Galactic black hole and neutron star) binary systems, but on much shorter time scales. For example, variability as short as $\sim$1–10 ms has been observed for the
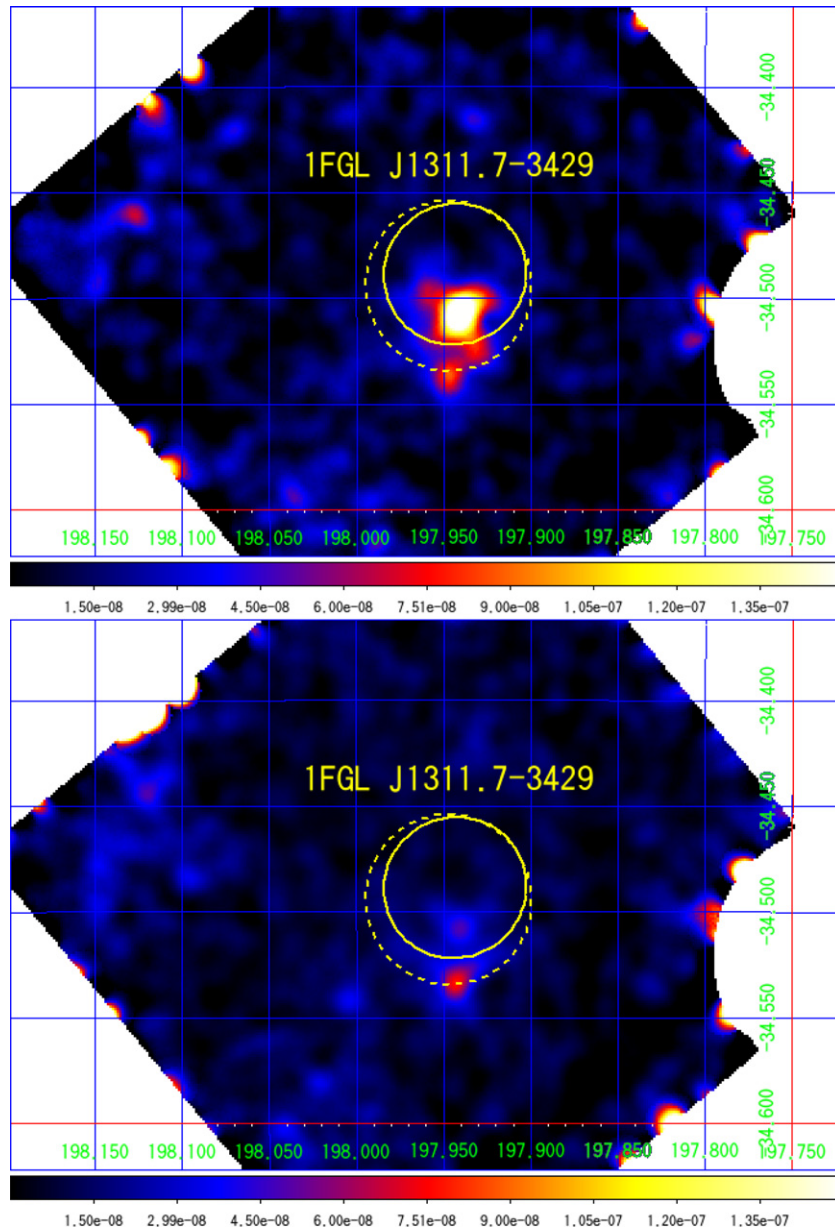
Figure 4. *Suzaku* XIS FI(XIS0+3) images of the 1FGL J1311.7−3429 region in the 0.5–10 keV photon energy range using the data during the first 20 ks (top; flare) and the last 74 ks (bottom; after the flare) in the 2009 observation obtained in AO4. The image shows the relative excess of smoothed photon counts (arbitrary units indicated in the color bar) and is displayed with linear scaling. The thick solid ellipse denotes the 95% position error of 1FGL J1311.7−3429 in the 2FGL catalog, while the dashed ellipse shows that reported in the 1FGL catalog. Note that the faint source to the south presented (and denoted as src B) in Maeda et al. (2011) is outside the 2FGL error circle.
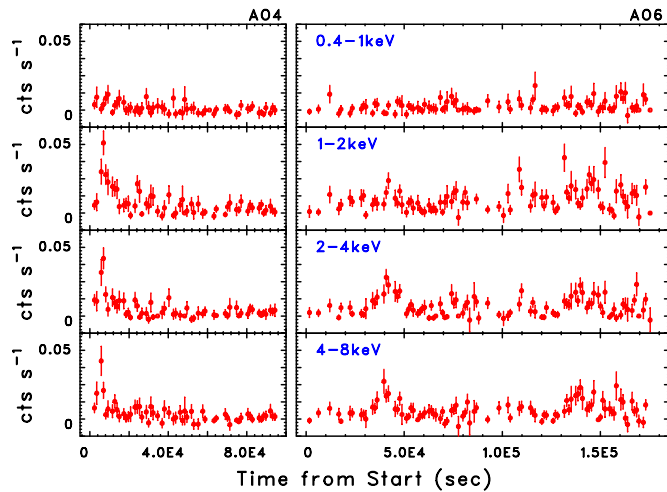
(A color version of this figure is available in the online journal.)

famous Galactic black hole source Cyg X-1 (e.g., Meekins et al. 1984; Hayashida et al. 1998).

Significant variability has also been observed in the optical (g', Rc, r'), where it is rather a quasi-sinusoidal flux modulation with a 1.56 hr period, as recently reported by Romani (2012). Moreover, we also found that the modulation profile, including the amplitude of modulation and peak intensity, has changed largely among the six nights of observations. The apparent modulation of magnitude observed in both the IAO and LOT data is quite similar to those observed in 1FGL J2339.7−0531, which is characterized by a 4.63 hr orbital period in optical and X-ray data (Romani & Shaw 2011; Kong et al. 2012). Note that 1FGL J2339.7−0531 is now suggested to be a "radio-quiet" gamma-ray emitting black-widow MSP with a $\simeq 0.1\,M_\odot$

late-type companion star, viewed at inclination $i \simeq 57°$. More-over, this compact object companion in 1FGL J2339.7−0531 is strongly heated, with $T_{\rm eff}$ varying from ~6900 K (superior conjunction) to <3000 K at minimum (Romani & Shaw 2011).

In this context, the spectral energy distribution (SED) of 1FGL J1311.7−3419 from radio to gamma-rays (Figure 9, top) may provide some hints on the nature of this mysterious source. 1FGL J1311.7−3419 has been the subject of both radio pulsar counterpart searches and blind searches for gamma-ray pulsations, but to date no pulsed emission has been detected (Ransom et al. 2011), and the situation is quite similar to the case for 1FGL J2339.7−0531. There are no NVSS radio sources catalogued within the 2FGL ellipse of 1FGL J1311.7−3429 down to 1.4 GHz flux completeness limit of $\simeq 2.5$ mJy

Figure 5. Multi-band *Suzaku* X-ray light curves of 1FGL J1311.7-3429 obtained during AO4 (2009) and AO6 (2011) observations: 0.4–1 keV, 1–2 keV, 2–4 keV, and 4–8 keV (from top to bottom). The XIS-0, 1, 3 data are summed.
(A color version of this figure is available in the online journal.)

(Condon et al. 1998), which is given as an arrow in Figure 9 (top). From the 0.1–100 GeV gamma-ray flux listed in the 2FGL catalog, $F_\gamma \equiv F_{0.1-100\,\text{GeV}} \simeq 6.2 \times 10^{-11}$ erg cm^{-2} s^{-1}, we obtain $F_\gamma/F_X \simeq 300$, $F_\gamma/F_R \gtrsim 1.7 \times 10^6$ for 1FGL J1311.7-3429, where F_X and F_R are the X-ray and radio fluxes measured in 2–10 keV and at 1.4 GHz, respectively. Note, these values are almost comparable to those measured in 1FGL J2339.7-0531, with $F_\gamma \simeq 3.0 \times 10^{-11}$ erg cm^2 s^{-1}, $F_\gamma/F_X \simeq 150$ and $F_\gamma/F_R \gtrsim 8.7 \times 10^5$. Although its flat spectrum X-ray continua and relatively high γ-ray-to-X-ray energy flux ratio (of $\gtrsim 100$) is typical of the subclass of blazars (FSRQ; Nolan et al. 2012), the non-detection in the radio as well as its curved gamma-ray spectrum seems to strongly disfavor an AGN association for 1FGL J1311.7-3429.

To further support the MSP association of 1FGL J1311.7-3429, Figure 9 (bottom) shows a close-up of the SED of 1FGL J1311.7-3429 in the optical/UV bands, reconstructed from IAO and *Swift* UVOT data. Observed magnitudes were converted to flux density based on Fukugita et al. (1995). Red dashed line indicates a tentative fit with a blackbody model of $T \simeq 1.2 \times 10^4$ K (or $kT \simeq 1$ eV) assuming an emission volume radius of $R_{bb} \simeq 1.5 \times 10^4 \, d_{kpc}$ km, where d_{kpc} is the distance to the source in units of 1 kpc. Therefore, the optical/UV spectrum of 1FGL J1311.7-3429 seems compatible with what is expected from a companion star of a radio-quiet MSP like 1FGL J2339.7-0531. A slightly higher temperature than 1FGL J2339.7-0531 ($kT \simeq 0.3$–0.6 keV; Romani & Shaw 2011) may indicate $\times 2$ smaller orbital radius, $\sim 5 \times 10^5$ km, for the 1FGL J1311.7-3429 binary system, assuming that the mass of the companion star is 0.1 $M_\odot$ and the pulsar spin-down luminosity is $L \simeq 10^{34}$ erg s^{-1} (parameters suggested for 1FGL J2339.7-0531 binary system; Romani & Shaw 2011). A change of the modulation profile observed in the r' band may be accounted for by rapid changes in the companion star temperature, but this remains uncertain.

Since both the optical and X-ray light curves in the case of 1FGL J2339.7-0531 clearly exhibits a 4.63 hr orbital modulation (Romani & Shaw 2011; Kong et al. 2012), the detection of periodicity in the X-ray light curve of 1FGL J1311.7-3429 is also likely. In fact, the folded X-ray light curve exhibits an excess feature around $\phi = 0.5$. As indicated by Romani (2012), this is presumably a pulsar superior conjunction, although both the
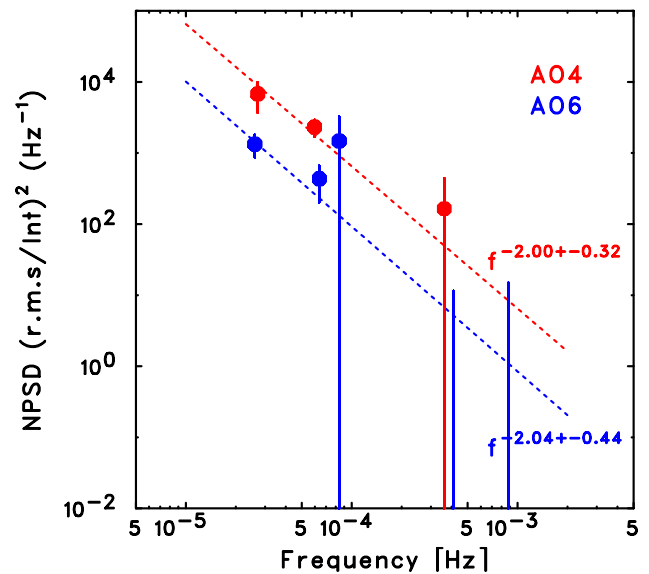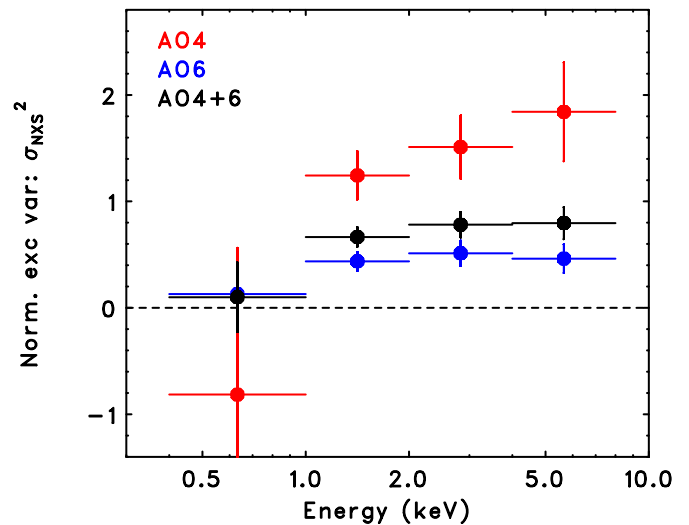

Figure 6. (Top) Energy dependence of X-ray variability of 1FGL J1311.7-3429. The variability parameter, excess variance was calculated for the total exposures in AO4 (2009; red) and AO6 (2011; blue) in four energy bands (see Figure 5). (Bottom) Normalized PSD (NPSD) calculated from the X-ray light curves of 1FGL J1311.7-3429. The dotted line shows the best-fitting power-law function of $\propto f^{-2.0}$.
(A color version of this figure is available in the online journal.)

normalized intensity as well as the phase peak appear to have changed substantially between the 2009 (AO4) and 2011 (AO6) observations. We therefore expect that X-ray variability consists of at least two different components—one associated with the binary motion as for the optical data, and the other a rather random fluctuation well represented by the NPSD of $P(f) \propto f^{-2}$, whose physical origin is still unknown but possibly related with perturbations associated with shock acceleration.

Such flaring X-ray variability has not yet been observed for 1FGL J2339.7-3429, but solely in 1FGL J1311.7-3429. In a review of X-ray emission from MSPs, Zavlin (2007) describes three primary sources of X-ray emission: (1) intrabinary shock, (2) the neutron star (NS) itself, and (3) pulsar wind nebula outside the binary system (see also Archibald et al. 2010). In fact, thermal emission of $kT \sim 0.1$–0.2 keV is often observed from MSPs, which is thought to arise from the surface of the NS and is steady with time (e.g., Marelli et al. 2011; Maeda et al. 2011). More recently, thermal emission of $kT \simeq 0.1$ keV was
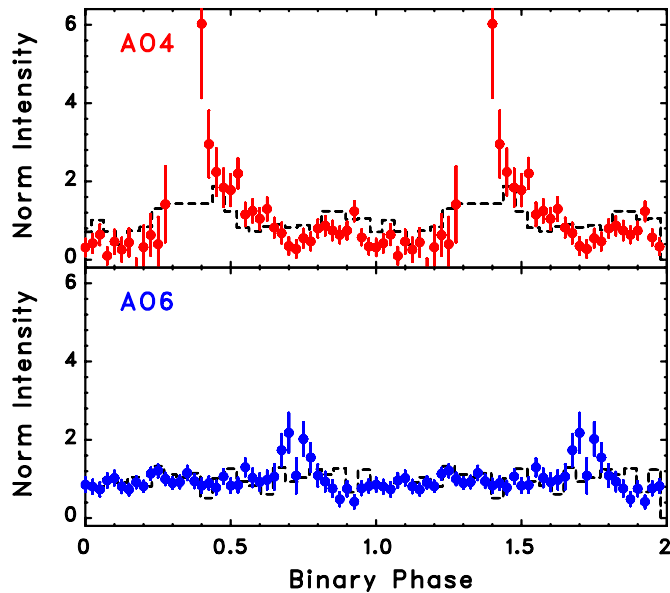
Figure 7. Folded X-ray light curves of 1FGL J1311.7-3429 reconstructed from the XIS data taken in *Suzaku* AO4 (top; red) and AO6 (bottom) observations. All the XIS0, 1, and 3 data are summed in the energy range of 0.4–10 keV. The phase zero is defined as MJD 56010.76808. The vertical axis represents the source counts divided by the average source intensity in the frame. The dashed line represents the folded X-ray light curves of a nearby field source (src B in Maeda et al. 2011) to confirm that observed excess is not due to artifacts caused by orbital gaps in the *Suzaku* data.
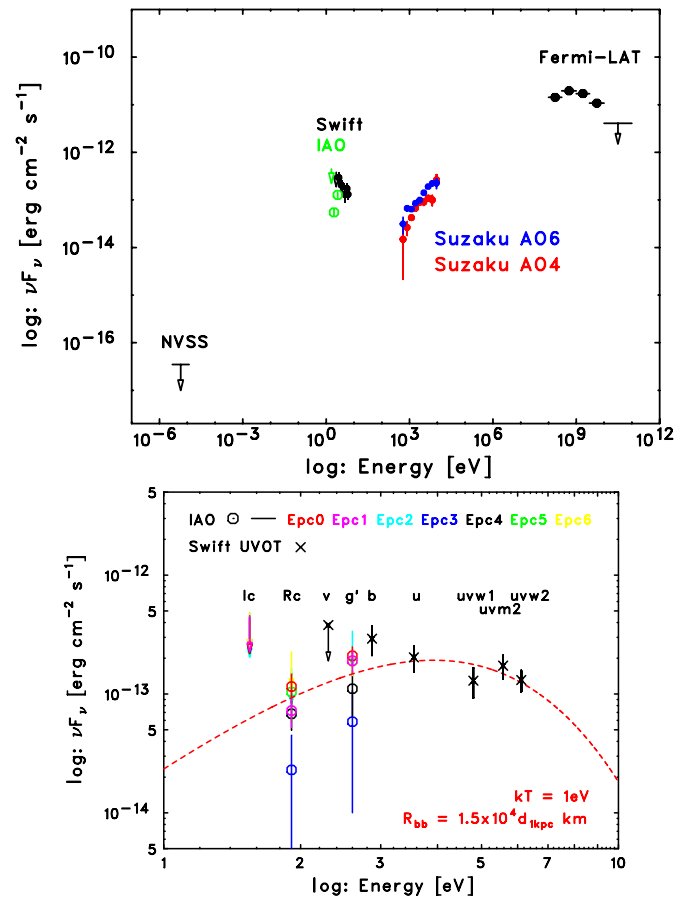
(A color version of this figure is available in the online journal.)
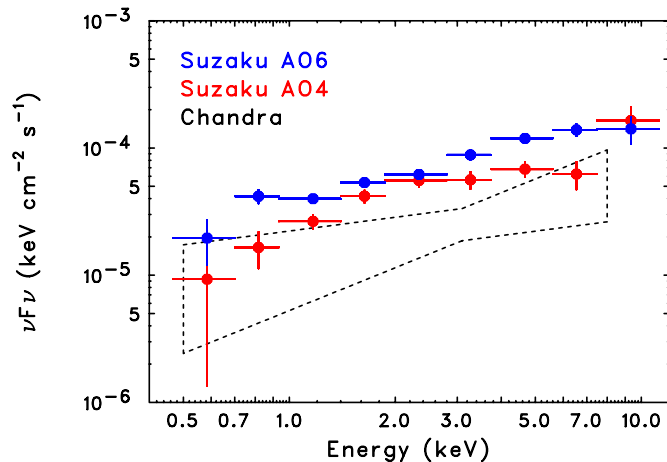
Figure 8. Comparison of the average X-ray spectra of 1FGL J1311.7-3429 observed in 2009 (AO4; red) and 2011 (AO6; blue) *Suzaku* observations. The X-ray data points represent the weighted mean of XIS0, 1, and 3. In addition, a bow-tie shows the best-fit parameters of the corresponding *Chandra* source, CXOU J131145.7-343030, observed in 2010 (Cheung et al. 2012).

(A color version of this figure is available in the online journal.)


Figure 9. (Top) Broadband spectrum of 1FGL J1311.703429. The X-ray data are as presented in Figure 8. The gamma-ray data points are taken from the 2FGL catalog (Nolan et al. 2012). The radio upper limit of 2.5 mJy at 1.4 GHz is taken from the NVSS catalog (Condon et al. 1998). The optical and UV data represents *Swift* UVOT data (see Maeda et al. 2011 and Cheung et al. 2012). (Bottom) Close-up of the broadband spectrum in the optical–UV range. Epochs 0–6 (1200 s each) correspond to time ranges defined in Figure 2. Note that the optical–UV spectrum is well fitted by a blackbody model of $kT \sim 1$ eV with a radius of the emission volume of $R_{bb} \simeq 1.5 \times 10^4 \, d_{kpc}$ km, where d_{kpc} is distance to the source in unit of 1 kpc.

(A color version of this figure is available in the online journal.)

also detected from 1FGL J2339.7-0531 (Kong et al. 2012, in prep), which is again steady despite the large flux modulation associated with binary motion being observed above 2 keV. Therefore, the fact that X-ray variability is not clearly seen below 1 keV may suggest that there could be some contribution from the surface of the NS, although from the spectral fitting it is not statistically significant. Then the variable, hard X-ray emission could arise from the intrabinary shock rather than the nebula because variability as short as $\simeq$10 ks is unlikely to originate

from the extended pulsar wind nebula.[11] Such a shock could readily produce gamma-ray emission (Arons & Tavani 1993). If localized, it could easily account for the orbital modulation as seen in the X-ray emission from 1FGL J2339.7-0531. But if material leaving the companion star, either through Roche lobe overflow or a stellar wind is non-uniform or patchy, we might expect random flaring activity as we see in the X-ray data of 1FGL J1311.7-3429.

We can also speculate on the nature of 1FGL J1311.7-3429 based solely on the gamma-ray properties, an approach already applied to the 1FGL unIDs in Ackermann et al. (2012). Figure 10 (top) presents a comparison of the 2FGL associated (either AGNs (blue) or PSRs (green)) and unassociated sources (red) in the VARIABILITY_INDEX and SIGNIF_CURVE plane. Apparently, 1FGL J1311.7-3429 is situated in the typical PSR regions of this diagnostic plane. Similarly, Figure 10 (bottom) plots the distribution of PSRs and AGNs in the PHOTON INDEX versus $F_{0.1-100 \, GeV}$ plane. In this case, 1FGL J1311.7-3429 is at

---

[11] Variability has been observed in some pulsar wind nebula in X-rays and gamma-rays, but with typical timescales of a week to months (e.g., Pavlov et al. 2001; Abdo et al. 2011).
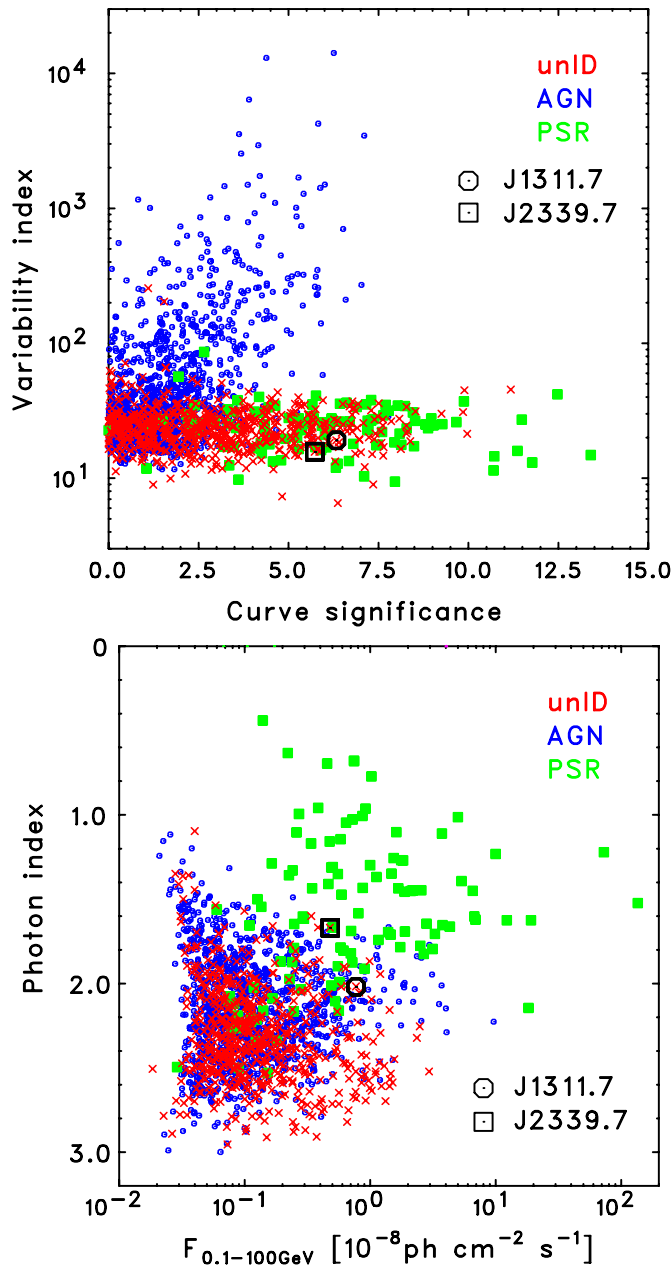
Figure 10. (Top) Comparison of the 2FGL Variability Index vs. Curvature Significance for associated sources (AGN: blue, PSR: green) and unassociated sources (red). (Bottom) Comparison of the 2FGL Photon Index vs. 0.1–100 GeV Flux for the associated sources and unassociated sources. In both panels, a separation between the AGN and PSR populations is evident. Note that 1FGL J1311.7-3429 is situated in the typical PSR region in the top panel, whilst at the boundary of AGN/PSR sources in the bottom panel.

(A color version of this figure is available in the online journal.)

the boundary of AGN and PSR sources, so is still consistent with a PSR association. For comparison, we also plot the gamma-ray parameters for 1FGL J2339.7-0531. In both panels, the gamma-ray properties of 1FGL J1311.7-3429 and 1FGL J2339.7-0531 are quite similar. Again, this supports the idea that 1FGL J1311.7-3429 is a black-widow system and may be a second example of a "radio-quiet" MSP after 1FGL J2339.7-0531.

Finally, if the rapid X-ray flaring variability observed with *Suzaku* may be due to inhomogeneity of shock material and/or

rapid changes in the beaming factor, this could be expected to occur also in gamma-rays, as suggested by a smooth connection of the spectrum between X-ray and gamma-ray energies. Moreover, we may see correlated variability also in the optical, which may be related to the change of modulation profile in the r'-band magnitudes that we see in Figure 3. Unfortunately, such fast variability is difficult to observe in gamma-rays as we mentioned for the one-month binned light curve in Section 1, despite the excellent sensitivity of *Fermi*-LAT. The low gamma-ray statistics also make it difficult to run a cross-correlation in order to measure any possible correlated optical, X-ray and gamma-ray variability. Further continuous investigation is necessary to confirm the origin of "variable" X-ray emission observed in the 1FGL J1311.7-3429 system.

REFERENCES

Abdo, A. A., Ackermann, M., Ajello, M., et al. 2009a, Science, 325, 848
Abdo, A. A., Ackermann, M., Ajello, M., et al. 2009b, ApJ, 706, L1
Abdo, A. A., Ackermann, M., Ajello, M., et al. 2009c, ApJ, 706, L56
Abdo, A. A., Ackermann, M., Ajello, M., et al. 2009d, ApJ, 701, L123
Abdo, A. A., Ackermann, M., Ajello, M., et al. 2009e, Science, 326, 1512
Abdo, A. A., Ackermann, M., Ajello, M., et al. 2009f, ApJS, 183, 46
Abdo, A. A., Ackermann, M., Ajello, M., et al. 2010a, ApJ, 710, L92
Abdo, A. A., Ackermann, M., Ajello, M., et al. 2010b, Science, 327, 1103
Abdo, A. A., Ackermann, M., Ajello, M., et al. 2010c, ApJ, 712, 459
Abdo, A. A., Ackermann, M., Ajello, M., et al. 2010d, ApJ, 713, 154
Abdo, A. A., Ackermann, M., Ajello, M., et al. 2010e, ApJ, 714, 927
Abdo, A. A., Ackermann, M., Ajello, M., et al. 2010f, Science, 329, 817
Abdo, A. A., Ackermann, M., Ajello, M., et al. 2010g, A&A, 512, 7
Abdo, A. A., Ackermann, M., Ajello, M., et al. 2010h, ApJ, 709, L152
Abdo, A. A., Ackermann, M., Ajello, M., et al. 2010i, Science, 328, 725
Abdo, A. A., Ackermann, M., Ajello, M., et al. 2010j, ApJS, 188, 405
Abdo, A. A., Ackermann, M., Ajello, M., et al. 2011, Science, 331, 739
Ackermann, M., Ajello, M., Allafort, A., et al. 2012, ApJ, 753, 83
Archibald, A. M., Kaspi, V. M., Bogdanov, S., et al. 2010, ApJ, 722, 88
Arons, J., & Tavani, M. 1993, ApJ, 403, 249
Atwood, W. B., Abdo, A. A., Ackermann, M., et al. 2009, ApJ, 697, 1071
Casandjian, J.-M., & Grenier, I. A. 2008, A&A, 489, 849
Cheung, C. C., Donato, D., Gehrels., N., et al. 2012, ApJ, 756, 33
Condon, J. J., Cotton, W. D., Greisen, E. W., et al. 1998, AJ, 115, 1693
Fukugita, M., Shimasaku, K., & Ichikawa, T. 1995, PASP, 107, 945
Hartman, R. C., Bertsch, D. L., Bloom, S. D., et al. 1999, ApJS, 123, 79
Hayashida, K., Miyamoto, S., Negoro, H., et al. 1998, ApJ, 500, 642
Huang, K. Y., Urata, Y., Filippenko, A. V., et al. 2005, ApJ, 628, L93
Kataoka, J., Reeves, J. N., Iwasawa, K., et al. 2007, PASJ, 59, 279
Kataoka, J., Takahashi, T., Wagner, S. J., et al. 2001, ApJ, 560, 659
Kong, A. K. H., Huang, R. H. H., Cheng, K. S., et al. 2012, ApJ, 747, L3
Maeda, K., Kataoka, J., Nakamori, T., et al. 2011, ApJ, 729, 103
Marelli, M., De Luca, A., & Caraveo, P. A. 2011, ApJ, 733, 82
Meekins, J. F., Wood, K. S., Hedler, R. L., et al. 1984, ApJ, 278, 288
Monet, D. G., Levine, S. E., Canzian, B., et al. 2003, AJ, 125, 948
Muslimov, A. G., & Harding, A. K. 2003, ApJ, 588, 430
Nolan, P. L., Abdo, A. A., Ackermann, M., et al. 2012, ApJS, 199, 31
Pavlov, G. G., Kargaltsev, O. Y., Sanwal, D., et al. 2001, ApJ, 554, L189
Ransom, S. M., Ray, P. S., Camilo, F., et al. 2011, ApJ, 772, L16
Romani, R. W. 2012, ApJ, 754, L25
Romani, R. W., & Shaw, M. S. 2011, ApJ, 743, L26
Sesar, B., Svilkovic, D., Ivezić, Ž., et al. 2006, AJ, 131, 2801
Takahashi, Y., Kataoka, J., Nakamori, T., et al. 2012, ApJ, 747, 64
Vaughan, S., Edelson, R., Warwick, R. S., & Uttley, P. 2003, MNRAS, 345, 1271
Zavlin, V. E. 2007, Ap&SS, 308, 297